

# A Physical Model for Drain Noise in High Electron Mobility Transistors: Theory and Experiment

Bekari Gabritchidze<sup>1b</sup>, Kieran A. Cleary<sup>1b</sup>, Anthony C. Readhead<sup>1b</sup>, Austin J. Minnich<sup>1b</sup>

**Abstract**—We report the on-wafer characterization of  $S$ -parameters and microwave noise temperature ( $T_{50}$ ) of discrete metamorphic GaAs high electron mobility transistors (HEMTs) at 40 K and 300 K over a range of drain-source voltages ( $V_{DS}$ ). From these data, we extract a small-signal model and the drain noise temperature ( $T_d$ ) at each bias and temperature. We find that  $T_d$  follows a superlinear trend with  $V_{DS}$  at both temperatures. These trends are interpreted by attributing drain noise to a thermal component associated with the channel resistance and a component due to real-space transfer (RST) of electrons from the channel to the barrier [1]. In the present devices at the minimum  $T_{50}$ , RST contributes  $\sim 10\%$  of the drain noise at cryogenic temperatures. At 300 K, the contribution increases to over  $\sim 60\%$  of the total drain noise. This finding indicates that improving the confinement of electrons in the quantum well could enable room-temperature receivers with up to  $\sim 50\%$  lower noise temperatures by decreasing the contribution of RST to drain noise.

**Index Terms**—High electron mobility transistors, cryogenic electronics, microwave noise, low-noise amplifiers, drain temperature, real-space transfer

## I. INTRODUCTION

HIGH electron mobility transistors are widely employed in microwave amplifiers due to their low noise characteristics [2], [3], [4]. While significant improvements have been made in their noise and frequency performance in past decades [5], [6], [7], [8], a physics-based understanding of the origin of microwave noise is lacking. Presently, noise in HEMTs is interpreted with the Pospieszalski model [9] in which noise is described using two uncorrelated noise generators associated with the gate and drain resistances  $R_{gs}$ ,  $R_{ds}$  with equivalent temperatures  $T_g$ ,  $T_d$ , respectively.  $T_g$  is modelled as the physical temperature ( $T_{ph}$ ) of the gate, while  $T_d$  is used as a fitting parameter and is on the order of 1000 K. Despite the utility of this model, it is unable to provide insight into the physical origin of  $T_d$ .

A recent theory attributes drain noise to microwave partition noise arising from real-space transfer (RST) [1]. In this mechanism, electrons are heated by the electric field under the

gate to physical temperatures exceeding 1000 K, a temperature sufficiently high that some electrons may thermionically emit out of the channel into the barrier. Because the barrier mobility is substantially less than that of the channel, two dissimilar conduction pathways exist from source to drain, creating partition noise. The theory makes several predictions, among them the dependence of  $T_d$  on physical temperature. A recent study using on-wafer characterization of discrete HEMTs observed the predicted temperature dependence of  $T_d$  [10], and other works have reported similar trends [11], [12], [13]. Additional dependencies of  $T_d$  have been observed experimentally, such as dependence on  $I_{DS}$  [11], [14], [15], [16] and  $V_{DS}$  [11], [16]. Despite these various experimental observations, the physical origin of drain noise in HEMTs remains a topic of debate.

In this paper, we performed on-wafer  $S$ -parameter and microwave noise measurements of discrete metamorphic GaAs HEMTs at 40 K and 300 K and various  $V_{DS}$  using a cryogenic probe station [17]. At each temperature and bias we extracted a small signal model (SSM) and obtained  $T_d$  by fitting the modeled and measured microwave noise ( $T_{50}$ ) at a generator impedance of 50  $\Omega$ . We find that  $T_d$  must depend on  $V_{DS}$  and  $T_{ph}$  to explain the measured  $T_{50}$  trends. These dependencies can be explained by considering drain noise to originate from a thermal component associated with the physical electron temperature in the channel, and another component arising from RST that depends exponentially on  $V_{DS}$  and  $T_{ph}$ . This analysis indicates that while RST contributes a small proportion of the noise at the typical low noise bias at cryogenic temperatures, it contributes around half of the total noise at 300 K. We use this finding to predict the noise temperatures that may be realized under various conditions if RST is suppressed.

This paper is organized as follows. A brief description of the experimental set up and the modeling is presented in Section II. The  $S$ -parameter and microwave noise characterization and the extracted drain temperatures are presented in Section III. A model for drain temperature is presented in Section IV, followed by a discussion of its implications in Section V. Finally, we provide a summary of the paper in Section VI.

## II. ON WAFER CRYOGENIC CHARACTERIZATION AND MODELING

The  $S$ -parameters and the microwave noise temperature of metamorphic GaAs HEMTs (OMMIC, D007IH, 4F50, gate length  $L_g = 70$  nm) were measured using a cryogenic probe station [17]. Further details of the measurement procedure are

This work was supported by the National Science Foundation under Grant No. 1911220. (Corresponding author: A. Minnich)

B. Gabritchidze is with the Division of Physics, Mathematics and Astronomy, California Institute of Technology, Pasadena, CA, 91125, and also with the Department of Physics, University of Crete, GR-70013 Heraklion, Greece (bekari@caltech.edu)

K. A. Cleary and A. C. Readhead are with the Division of Physics, Mathematics and Astronomy, California Institute of Technology, Pasadena, CA, 91125. (kcleary@astro.caltech.edu, acr@astro.caltech.edu)

A. J. Minnich is with Division of Engineering and Applied Science, California Institute of Technology, Pasadena, CA, 91125 (aminnich@caltech.edu)

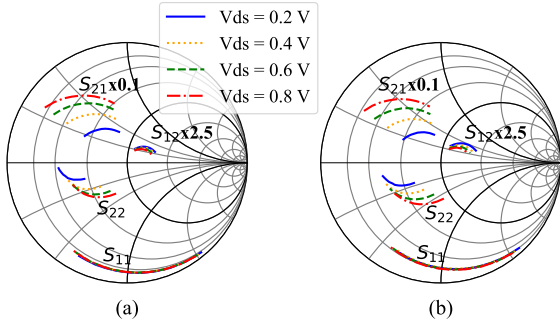


Fig. 1: Measured  $S$ -parameters versus frequency over 5 – 15 GHz at various  $V_{DS}$  and physical temperatures of 40 K (a) and 300 K (b).

given in [10]. In brief, the  $S$ -parameter measurements were carried out in the frequency range 5 – 15 GHz using a vector network analyzer (VNA, Rhode & Schwartz ZVA50). The system was calibrated by transferring the measurement plane from the VNA to the tips of the wafer probes (GGB industries, 40A-GSG-100-DP) by through-reflect-match calibration on a CS-5 calibration substrate (GGB Industries).

The microwave noise was measured using the Y-factor method with a cold attenuator [18] at a generator impedance of  $50 \Omega$ . 10 dB cryogenic and room temperature attenuators (Quantum Microwave) were inserted between the noise source (Keysight, N4002A) and the device under test (DUT). The room temperature attenuator was connected directly to the noise source (NS) to reduce the change in output reflections from the ‘on’ to ‘off’ state of the NS, while the cryogenic attenuator was connected to the RF probe contacting the input of the DUT and served as a cold load. After the DUT, a cryogenic amplifier (Cosmic Microwave, CIT1-18) was used inside the probe station, and a combination of mixer, oscillator, filters, amplifiers and a power sensor were used outside the probe station to further process and measure the incident noise power. With the  $S$ -parameter and  $T_{50}$  measurements, a small-signal model (SSM) was generated by direct extraction and optimization of the intrinsic parameters. A noise model was obtained by fitting the measured and modeled  $T_{50}$  using the drain temperature,  $T_d$ , as a fitting parameter.

### III. EXPERIMENTAL RESULTS

Fig. 1 shows the measured  $S$ -parameters at various  $V_{DS}$  ranging from 0.2 – 0.8 V and physical temperatures of 40 K and 300 K. At a given  $T_{ph}$ ,  $S_{21}$  and  $S_{22}$  exhibit the largest variation with  $V_{DS}$ , while  $S_{12}$  and  $S_{11}$  show smaller but observable dependence.

In Fig. 2,  $T_{50}$  versus frequency is shown for various  $V_{DS}$  and the two physical temperatures. The error bars were determined by propagating the uncertainties of the measurement setup, from the noise source to the power meter, through the computation of Y-factor. The uncertainties in  $T_{50}$  are dominated by uncertainty in the measured microwave power as well as systematic uncertainties in the values of the insertion

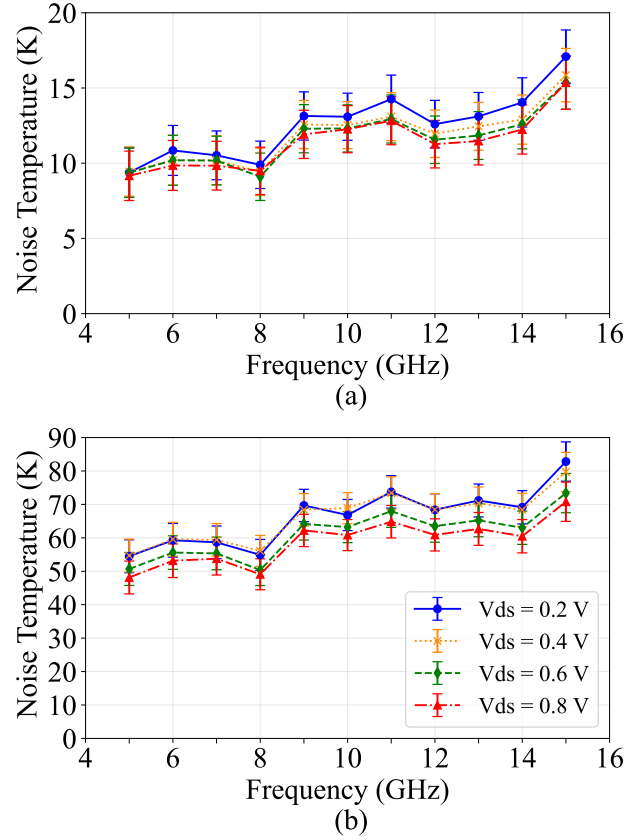


Fig. 2: Measured  $T_{50}$  versus frequency at various  $V_{DS}$  and physical temperature of 40 K (a) and 300 K (b).

loss (IL),  $\sim 0.1$  dB, of the coaxial components at cryogenic temperatures. The repeatability of  $T_{50}$  was found to be  $\sim 1$  K. In both the  $S$ -parameter and noise measurements, the gate voltage ( $V_{GS}$ ) was kept constant,  $V_{GS} = -136$  mV at  $T_{ph} = 40$  K, and  $V_{GS} = -226$  mV at  $T_{ph} = 300$  K, for all  $V_{DS}$ . These  $V_{GS}$  were selected so that  $I_{DS} = 20$  mA at  $V_{DS} = 0.8$  V and a given  $T_{ph}$ .

Figs. 3a and 3b show  $T_{50}$  and the transconductance ( $g_m$ ) versus  $V_{DS}$  at 12 GHz, for physical temperatures of 40 K and 300 K. Similar trends are observed at both temperatures, with the minimum in  $T_{50}$  shifting from  $V_{DS} \sim 0.8$  V at 300 K to  $V_{DS} \sim 0.5$  V at 40 K. This observation is explained by higher  $g_m$  at  $T_{ph} = 40$  K than at 300 K for a given  $V_{DS}$  and therefore reduced contribution of drain noise to  $T_{50}$ . The transconductance  $g_m$  increases with increasing  $V_{DS}$  but plateaus at  $V_{DS} \gtrsim 1.0$  V and both  $T_{ph}$ .

Qualitative findings can be obtained from the trend of  $g_m$  and  $T_{50}$  versus  $V_{DS}$ . In particular, as  $V_{DS}$  increases above 0.6 V, both  $g_m$  and  $T_{50}$  increase. Assuming that self-heating effects can be neglected, the increase in  $T_{50}$  despite the increased gain must arise from  $T_d$ , indicating that  $T_d$  exhibits a dependence on  $V_{DS}$ . This dependence cannot be attributed to non-ideal effects like impact ionization, as at all  $V_{DS}$  and  $V_{GS}$  values the gate-source current,  $I_{GS}$ , remained at values between  $-1 \mu\text{A}$  and  $-10 \mu\text{A}$ . However, impact ionization is often accompanied by a marked increase in gate current (see

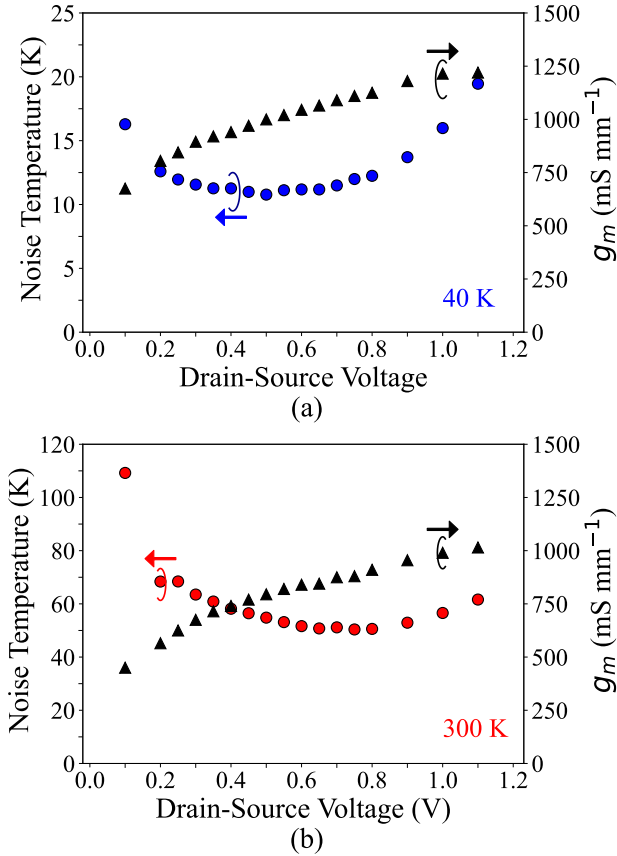


Fig. 3: Measured  $T_{50}$  (left y-axis, blue circles) at 12 GHz and transconductance  $g_m$  (right y-axis, black triangles) at  $T_{ph}$  of 40 K (a) and 300 K (b). Measured  $T_{50}$  and  $g_{ds}$  versus physical temperature.

[4, Fig. 1] and [19, Fig. 6.7]) and occurs in different bias regime than employed here ( $V_{GS} > 0$  V,  $V_{DS} > 1.0$  V) [19]. Therefore impact ionization is unlikely to be the origin of the variation of  $T_d$  with  $V_{DS}$ .

To gain quantitative insight, we extract  $T_d$  at each bias and temperature using the measured  $T_{50}$  and S-parameters. The extracted  $T_d$  versus  $V_{DS}$  at 40 K and 300 K is shown in Figs. 4a and 4b. Additional  $T_d$  measurements for a similar device from the same wafer reticle are also shown at selected  $V_{DS}$ . The extracted  $T_d$  follows a linear trend at low  $V_{DS} \lesssim 0.6$  V and rises super-linearly at higher voltages. The error bars for the extracted  $T_d$  were determined by calculating  $T_d$  for the minimum and maximum values of  $T_{50}$  within the error bars and were found to range from  $\pm 150$  K to  $\pm 400$  K, depending on physical temperature and the uncertainty in  $T_{50}$ .

At 40 K, we observe that the reduction of  $g_m$  in Fig. 3a with decreasing  $V_{DS}$  is accompanied by a non-monotonic variation in  $T_{50}$ . Specifically,  $T_{50}$  decreases with decreasing  $V_{DS}$  until a minimum ( $T_{50}^{min}$ ) is observed at  $\sim 0.5$  V and  $\sim 0.8$  V and 40 K and 300 K, respectively. The increase of  $T_{50}$  around its minimum is attributed to two different mechanisms. At bias below the low noise bias, the increase in noise with decreasing  $V_{DS}$  is due to reduced gain. At higher  $V_{DS}$ , both  $g_m$  and  $T_d$  increase with increasing  $V_{DS}$ , reaching maximum values of

$\sim 1250$  mS mm<sup>-1</sup> and  $\sim 2200$  K at  $V_{DS} = 1.1$  V, respectively. However, due to the more rapid increase of  $T_d$  for  $V_{DS} > 0.5$  V compared to that of  $g_m$ ,  $T_{50}$  exhibits an increase. A similar variation of  $g_m$ ,  $T_{50}$  and  $T_d$  with  $V_{DS}$  is observed at 300 K (Figs. 3b and 4b).

#### IV. PHYSICAL MODEL FOR DRAIN NOISE

The extracted drain temperatures exhibit a superlinear trend as a function of  $V_{DS}$  (Fig. 4) at both cryogenic and room temperatures. In our prior work [10] and other works [11], [12],  $T_d$  is also observed to depend superlinearly on physical temperature (data from [10] are reproduced in Fig. 5).

We now aim to interpret these trends through a theory of drain noise. A proposed mechanism for drain noise based on a suppressed shot noise theory was suggested in [20] in which  $T_d$  was expressed in terms of a temperature-independent suppression factor (Fano factor),  $g_{ds}$  and  $I_{DS}$ . According to this theory, if  $I_{DS}$  is kept constant with physical temperature then the output noise power  $T_d g_{ds}$  is predicted to be temperature independent. This prediction is inconsistent with the measured temperature dependence of the output noise power which changes from  $\sim 30$  pA(Hz mm)<sup>-1/2</sup> to  $\sim 45$  pA(Hz mm)<sup>-1/2</sup> as  $T_{ph}$  is varied from 40 K to 300 K. This conclusion is consistent with the findings of [10], [11], [12].

We now quantitatively interpret the measured trends of  $T_d$  in terms of the RST theory for drain noise proposed in [1]. This theory predicts  $T_d$  to exhibit an exponential dependence on  $T_{ph}$  and  $V_{DS}$ . However, the measured trends vary less rapidly than predicted from RST alone. We therefore introduce a model of drain noise based on earlier studies of microwave noise in quantum wells [21] in which the noise arises from two components: the thermal noise associated with the channel resistance and RST.  $T_d$  can then be expressed as:

$$T_d = T_e + T_{RST} \quad (1)$$

where the RST noise temperature is given as:

$$T_{RST} = T_{RST}^0 \exp[-(\Delta E_c - q(V_{GS} - V_{th}))/k_B T_e] \quad (2)$$

Here,  $q$  is the electric charge,  $k_B$  the Boltzmann constant,  $V_{GS}$  the gate-source voltage,  $V_{th}$  the threshold voltage, and  $\Delta E_c$  the channel-barrier conduction band discontinuity. The temperature dependence of  $\Delta E_c$  was omitted and was set to  $\sim 0.5$  eV at all  $T_{ph}$  [22]. From [1, eq. (4)],

$$T_{RST}^0 = q^2 v_{d1}^2 n_{s1} \tau \gamma W / k_B g_{ds} L_g, \quad (3)$$

where  $v_{d1} \sim 4 \times 10^7$  cm s<sup>-1</sup> is the saturation velocity in the channel [23],  $\tau \sim 1$  ps is the characteristic time of electrons to transfer from channel to barrier [24],  $n_{s1}$  is the channel electron sheet density (typically  $\sim 2 \times 10^{12}$  cm<sup>-2</sup> [21]),  $W$  is the gate width,  $g_{ds}$  the drain-source conductance extracted from the small-signal model,  $L_g \sim 70$  nm is the gate length, and  $\gamma$  is the probability of hot electrons to emit from channel to barrier. For simplicity, it is assumed that all electrons with energy exceeding  $\Delta E_c$  transfer to the barrier so that  $\gamma = 1$ , and that  $T_{RST}^0$  is independent of temperature. In the model, the difference  $V_{GS} - V_{th}$  was fixed at  $V_{GS} - V_{th} \sim 43$  mV so that at constant  $V_{DS} = 0.6$  V and all  $T_{ph}$  the  $I_{DS} = 10$

mA. The specific values of these parameters are of secondary importance since the trends of  $T_d$  versus  $V_{DS}$  and  $T_{ph}$  are the focus of the subsequent discussion.

Using (1), we solve for  $T_e$  and thereby obtain  $T_e$  and  $T_{RST}$ , corresponding to the thermal and RST components of  $T_d$ , respectively, at each extracted  $T_d$  of Fig. 4. The result is shown in Fig. 4. The obtained  $T_e$  increases with  $V_{DS}$ ; however, the rate of increase is reduced and plateaus at  $V_{DS} \gtrsim 1.0$  V. We observe that  $T_e$  and  $T_d$  differ by less than 10% for  $V_{DS} \lesssim 0.6$  V and  $T_{ph} = 40$  K, indicating that RST makes a minor contribution at these  $V_{DS}$ . At higher  $V_{DS}$  a marked deviation between  $T_d$  and  $T_e$  is observed, indicating the onset of the RST component. At 300 K,  $T_e$  is higher due to the higher  $T_{ph}$ , and as a result, RST starts to contribute to the total drain temperature even at  $V_{DS} \sim 0.2$  V.

Fig. 5 shows the temperature dependence of  $T_d$  at various  $T_{ph}$  from 40 K to 300 K at  $V_{DS} = 0.6$  V and  $I_{DS} = 10$  mA first reported in [10]. Following the same procedure, we are now able to separate the individual contributions of thermal and RST to  $T_d$ . A nearly linear dependence of  $T_e$  on  $T_{ph}$  is observed, as expected, but the RST temperature,  $T_{RST}$ , follows a superlinear trend with  $T_{ph}$ , varying from  $\sim 40$  K to  $\sim 1000$  K over the same physical temperature range. The total contribution of RST to  $T_d$  varies depending on  $V_{DS}$  as in Fig. 4; however, the RST contribution to drain noise increases monotonically and superlinearly as the physical temperature increases.

## V. DISCUSSION

We now consider our model for drain noise in the context of prior studies of microwave noise in HEMTs and quantum wells. Microwave noise in InGaAs quantum wells has been extensively studied as described in [21]. These devices can be regarded as ungated HEMTs. The measured noise was observed to exhibit a strong dependence on electric field above a certain threshold value which depended on the value of the conduction band offset between the channel and barrier ([21, Fig. 16.12] and [21, Fig. 17.1]), and these trends were attributed to the contribution of thermal noise and RST. The characteristics of the drain noise reported here and their interpretation are therefore consistent with these prior studies of microwave noise in III-V quantum wells.

With a physical model for drain noise, we estimate the magnitude of improvement in  $T_{50}$  if the RST contribution were suppressed by improved confinement of electrons in the quantum well. In Fig. 6a we plot the measured  $T_{50}$  as a function of  $T_{ph}$  at constant  $V_{DS} = 0.6$  V,  $I_{DS} = 10$  mA and frequency of 12 GHz. In this plot, we also show the predicted trend of  $T_{50}$  if RST were absent and drain noise was therefore due solely to thermal noise from the channel resistance. This curve is obtained by setting  $T_d = T_e$  in our noise model. We observe that under these bias conditions, the predicted  $T_{50}$  could vary linearly with  $T_{ph}$  rather than superlinearly, leading to relatively larger improvements in noise performance at room temperature compared to cryogenic temperature.

To examine this prediction in more detail, in Figs. 6b and 6c we plot the measured  $T_{50}$  and the  $T_{50}$  predicted if the

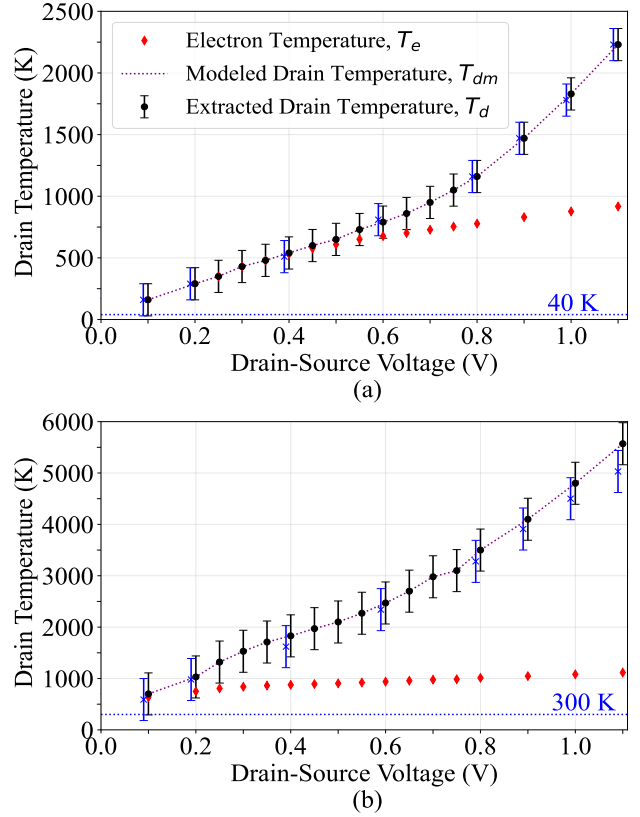


Fig. 4: Extracted  $T_d$  (black circles), electron physical temperature  $T_e$  (red diamonds) and drain-temperature  $T_{dm}$  (purple dotted line) based on (1) at 40 K (a) and 300 K (b) versus  $V_{DS}$ . The  $T_d$  is shown for an additional device from the same wafer reticle (blue crosses). One data set was shifted to the left by 10 mV to make the two data sets discernible. The physical temperature,  $T_{ph}$  is shown as a comparison in both (a) and (b) as dotted line parallel to  $V_{DS}$  axis.

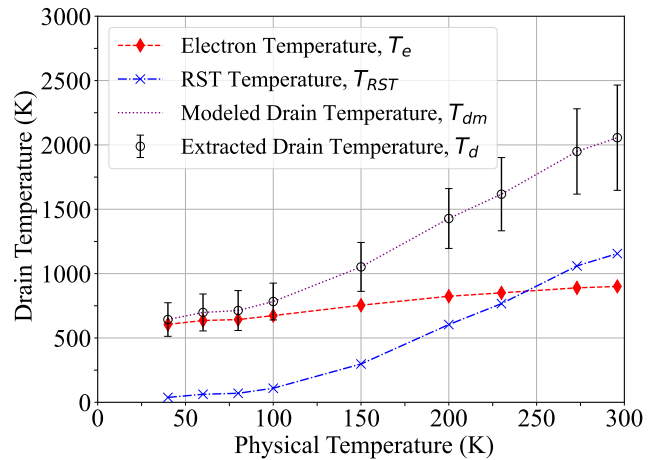


Fig. 5: Extracted drain temperature  $T_d$  (black circles) versus physical temperature  $T_{ph}$  at constant  $V_{DS} = 0.6$  V and  $I_{DS} = 10$  mA [10]. The electron physical temperature  $T_e$  (red dashed line and diamond marker) derived by solving (1); the real space transfer part  $T_{RST}$  of (1) (blue dashed dot line cross marker) and the modeled drain-temperature  $T_{dm}$  (dotted purple lines).



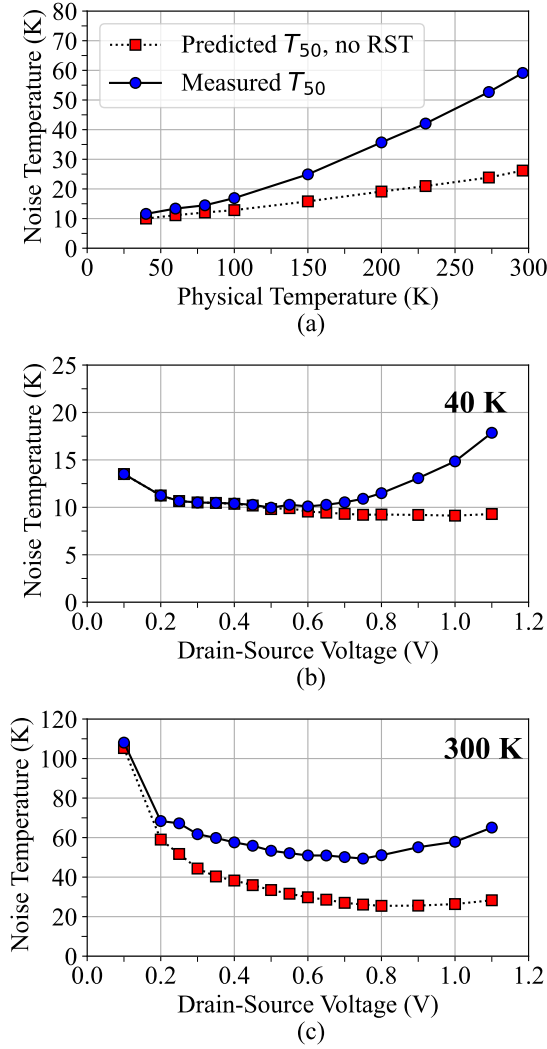


Fig. 6: Measured  $T_{50}$  [10] and predicted  $T_{50}$  versus physical temperature at constant  $V_{DS} = 0.6$  V and  $I_{DS} = 10$  mA (a), and versus  $V_{DS}$  at 40 K (b) and 300 K (c) at constant  $V_{GS} = -136$  mV and  $V_{GS} = -226$  mV, respectively. The predicted  $T_{50}$  is modeled by replacing the extracted  $T_d$  with  $T_e$  (i.e.  $T_{RST} = 0$ ) in the noise model. All the above data are at the frequency of 12 GHz. The  $V_{GS}$  in (b) and (c) were selected so that at both physical temperatures,  $V_{DS} = 0.8$  V and  $I_{ds} = 20$  mA.

contribution of RST to  $T_d$  were suppressed, versus  $V_{DS}$  at 40 K and 300 K, respectively. At 40 K, the measured and predicted  $T_{50}$  exhibit a negligible difference for  $V_{DS} \lesssim 0.6$  V, but at higher  $V_{DS}$  the predicted  $T_{50}$  is markedly less than the measured value owing to the lack of noise from RST. The minimum of  $T_{50}$  at 40 K would improve by  $\sim 5\%$  if RST were suppressed. At 300 K, the difference between measured and predicted  $T_{50}$  varies by up to  $\sim 60\%$  as  $V_{DS}$  is increased from 0.1 V to 1.1 V. In this case, the minimum  $T_{50}$  would improve by  $\sim 50\%$  in the absence of RST, suggesting that significant improvements in room temperature noise figure may be possible if RST is suppressed.

Finally, we discuss these findings in the context of ap-

plications of HEMTs in radio astronomy. To facilitate comparison, we assume all parameters are left unchanged except for removing RST from  $T_d$ . At cryogenic temperatures, RST appears to make a minor contribution in the present devices, and so suppressing RST would lead to  $\sim 5\%$  improvement in minimum  $T_{50}$  based on Fig. 6b. However, suppression of the RST component of  $T_d$  would allow the HEMT to be operated at higher gain without incurring a noise penalty. This would lead to improvement in gain by  $\sim 20\%$  and the overall receiver noise temperature could therefore be reduced further by suppressing the contribution of components after the cryogenic LNA. At 300 K, suppression of the RST component promises the potential to reduce the minimum  $T_{50}$  of the HEMT by up to 50%. This possibility has significant implications for the design and performance of large telescope arrays for radio astronomy that rely on ambient-temperature LNAs, such as the planned 2000-dish Deep Synoptic Array (DSA-2000; [25]). A reduction in LNA noise temperature by 50% for the DSA-2000 would have the effect of increasing its survey speed by around 75%, representing a major increase in performance achieved by the extremely cost-effective route of replacing the low noise amplifier. This potential is therefore a topic of interest for further investigation.

## VI. CONCLUSION

In summary, we have characterized the  $S$ -parameters and the microwave noise temperature of GaAs HEMTs at 40 K and 300 K and various  $V_{DS}$ . At each  $T_{ph}$  and  $V_{DS}$  we have extracted the drain temperature,  $T_d$ . From these data, we obtained the dependence of  $T_d$  on  $V_{DS}$  at 40 K and 300 K.  $T_d$  is found to exhibit a superlinear trend with  $V_{DS}$  at both temperatures. Specifically, the voltage dependence indicates a superlinear trend for  $V_{DS} \gtrsim 0.6$  V at 40 K and for  $V_{DS} \gtrsim 0.4$  V at 300 K. We have introduced a model capable of explaining these trends in which drain noise originates from thermal noise of the channel resistance and RST of electrons from the channel to the barrier. The analysis indicates that at cryogenic temperatures and typical low-noise biases, thermal noise from the channel resistance is the main component of  $T_d$  in the present devices, while at 300 K, RST accounts for over half of  $T_d$ . We used these findings to show that  $T_{50}$  can be improved by as much as 50% at 300 K if RST could be suppressed, for instance by improving the confinement of the electrons in the quantum well.

## ACKNOWLEDGMENT

The authors thank Sander Weinreb, Pekka Kangaslahti, Jun Shi, Junjie Li and Jan Grahn for useful discussions.

## REFERENCES

- [1] I. Esho, A. Y. Choi, and A. J. Minnich, "Theory of drain noise in high electron mobility transistors based on real-space transfer," *J. Appl. Phys.*, vol. 131, no. 8, p. 085111, Feb. 2022.
- [2] U. Mishra and J. Shealy, "InP-based HEMTs: status and potential," in *Proc. of Int. Conf. on Ind. Phos. and Rel. Mat.*, 1994, pp. 14–17.
- [3] E. Bryerton, M. Morgan, and M. Pospieszalski, "Ultra low noise cryogenic amplifiers for radio astronomy," in *2013 IEEE Radio Wireless Symp.*, Jan. 2013, pp. 358–360.

- [4] E. Cha, N. Wadefalk, G. Moschetti, A. Pourkabirian, J. Stenarson, and J. Grahn, "A 300- $\mu$ W Cryogenic HEMT LNA for Quantum Computing," in *IEEE MTT-S Int. Microw. Symp.*, Aug. 2020, pp. 358–360.
- [5] E. Cha, *et al.*, "0.314 and 1628 GHz Wide-Bandwidth Cryogenic MMIC Low-Noise Amplifiers," *IEEE Trans. Microw. Theory Tech.*, vol. 66, no. 11, pp. 4860–4869, 2018.
- [6] W. R. Deal, *et al.*, "Low noise amplification at 0.67 THz using 30 nm InP HEMTs," *IEEE Microw. Wirel. Compon. Lett.*, vol. 21, no. 7, pp. 368–370, 2011.
- [7] F. Thome, F. Schfer, S. Trk, P. Yagoubov, and A. Leuther, "A 67-116-GHz Cryogenic Low-Noise Amplifier in a 50-nm InGaAs Metamorphic HEMT Technology," *IEEE Microw. Wirel. Compon. Lett.*, pp. 1–4, 2021.
- [8] D. Cuadrado-Calle, *et al.*, "Broadband MMIC LNAs for ALMA Band 2+3 With Noise Temperature Below 28 K," *IEEE Trans. Microw. Theory Tech.*, vol. 65, no. 5, pp. 1589–1597, May 2017.
- [9] M. Pospieszalski, "Modeling of noise parameters of mesfets and modfets and their frequency and temperature dependence," *IEEE Trans. Microw. Theory Tech.*, vol. 37, no. 9, pp. 1340–1350, 1989.
- [10] B. Gabritchidze, K. Cleary, J. Kooi, I. Esho, A. C. Readhead, and A. J. Minnich, "Experimental characterization of temperature-dependent microwave noise of discrete HEMTs: Drain noise and real-space transfer," in *IEEE MTT-S Int. Microw. Symp. Dig.*, 2022, pp. 615–618.
- [11] F. Heinz, F. Thome, D. Schwantuschke, A. Leuther, and O. Ambacher, "A Scalable Small-Signal and Noise Model for High-Electron-Mobility Transistors Working Down to Cryogenic Temperatures," *IEEE Trans. Microw. Theory Tech.*, vol. 70, no. 2, pp. 1097–1110, Feb. 2022.
- [12] M. Murti, *et al.*, "Temperature-dependent small-signal and noise parameter measurements and modeling on InP HEMTs," *IEEE Trans. Microw. Theory Tech.*, vol. 48, no. 12, pp. 2579–2587, 2000.
- [13] S. Weinreb and J. Shi, "Low Noise Amplifier With 7-K Noise at 1.4 GHz and 25 C," *IEEE Trans. Microw. Theory Tech.*, vol. 69, no. 4, pp. 2345–2351, 2021.
- [14] M. W. Pospieszalski and A. C. Niedzwiecki, "FET noise model and on-wafer measurement of noise parameters," in *IEEE MTT-S Int. Microw. Symp. Dig.*, July 1991, pp. 1117–1120 vol.3, ISSN: 0149-645X.
- [15] J. Schlee, H. Rodilla, N. Wadefalk, P.-N. Nilsson, and J. Grahn, "Characterization and Modeling of Cryogenic Ultralow-Noise InP HEMTs," *IEEE Trans. Electron Devices*, vol. 60, pp. 206–212, Jan. 2013.
- [16] F. Heinz, F. Thome, A. Leuther, and O. Ambacher, "Noise Performance of Sub-100-nm Metamorphic HEMT Technologies," in *IEEE MTT-S Int. Microw. Symp.*, Aug. 2020, pp. 293–296.
- [17] D. Russell, K. Cleary, and R. Reeves, "Cryogenic probe station for on-wafer characterization of electrical devices," *Rev. Sci. Instrum.*, vol. 83, no. 4, p. 044703, 2012.
- [18] J. Fernandez, "A Noise Temperature Measurement System Using a Cryogenic Attenuator," *TMO Prog. Report*, no. 42, p. 135, 1998.
- [19] A. H. Akgiray, "New Technologies Driving Decade-Bandwidth Radio Astronomy: Quad-ridged Flared Horn and Compound-Semiconductor LNAs," Ph.D. dissertation, Cal. Inst. of Tech., Pasadena, CA, USA, 2013.
- [20] M. Pospieszalski, "On the limits of noise performance of field effect transistors," in *IEEE MTT-S Int. Microw. Symp.*, 2017, pp. 1953–1956.
- [21] H. Hartnagel, R. Katilius, and A. Matulionis, *Microwave Noise in Semiconductor Devices*, 1st ed. NY, USA: Wiley-Intersci. Ser., 2001.
- [22] F. Schwierz and J. J. Liou, *Modern Microwave Transistors: Theory, Design, and Performance*, 1st ed. NY, USA: Wiley-Intersci. Ser., 2002.
- [23] J. Schlee, "Ultra-Low Noise InP HEMTs for Cryogenic Amplification," Ph.D. dissertation, Chalm. Univ. of Tech., Got. Sweden, 2012.
- [24] B. K. Ridley, "Hot electrons in low-dimensional structures," *Rep. Prog. Phys.*, vol. 54, no. 2, pp. 169–256, 1991.
- [25] G. Hallinan, *et al.*, "The DSA-2000 – A Radio Survey Camera," 2019, arXiv:1907.07648.



as their employment in Monolithic Microwave Integrated Circuits.



he leads an effort to optimize the cryogenic performance of amplifiers for radio astronomy. He is also the Associate Director of the Owens Valley Radio Observatory.



the recipient of a 2019 Presidential Early Career Award for Scientists and Engineers.



Cavendish Laboratory, including 15 months as a Post-Doctoral Fellow with the California Institute of Technology. In 1977, he returned to the California Institute of Technology, where he was appointed to the professorial faculty there in 1981. He has held a number of positions with the California Institute of Technology, including Director of the Owens Valley Radio Observatory (1981-1986, 2007 present); Executive Officer of Astronomy (1990-1992; 2012-2013), and Director of the Chajnantor Observatory in Chile (2006-2009). His scientific interests have been focused on cosmology and active galaxies and on techniques of high-resolution astronomy and imaging.

**Bekari Gabritchidze** Bekari Gabritchidze received M.Sc degree in advanced physic from University of Crete, Department of Physics, Crete, Greece, in 2017. He is currently pursuing the Ph.D degree as a visiting student at Cahill Radio Astronomy Laboratory, California Institute of Technology, Pasadena, CA and will defend his thesis at the University of Crete, Department of Physics, Crete, Greece. His current research interest include low-noise High Electron Mobility Transistors (HEMTs), the design, modelling and characterization of HEMTs as well

**Kieran Cleary** Kieran A. Cleary received the M.Eng.Sc. degree in electronic engineering from the National University of Ireland, Dublin, in 1994, and the Ph.D. degree in radio astronomy (on cosmic microwave background observations using the very small array) from the University of Manchester, U.K. in 2004. He is currently a Senior Scientist at the California Institute of Technology, Pasadena, CA, leading a spectral line intensity mapping experiment (COMAP) targeting the Epoch of Galaxy Assembly. At the Cahill Radio Astronomy Laboratory (CRAL),

**Austin J. Minnich** Austin J. Minnich received the B.S. degree in engineering science from the University of California, Berkeley, CA, USA, in 2006, and the Ph.D. degree in Mechanical Engineering from the Massachusetts Institute of Technology, Cambridge, MA, USA, in 2011. He is currently a Professor of Mechanical Engineering and Applied Physics at the California Institute of Technology, Pasadena, CA, USA. His current research interests include low-noise semiconducting and superconducting devices for astrophysical applications. Prof. Minnich was

**Anthony C. Readhead** Anthony C. Readhead was born in South Africa. He received the B.Sc and B.Sc (Hons) degrees from the University of the Witwatersrand, Johannesburg, South Africa, and the Ph.D. degree from the Cavendish Laboratory, University of Cambridge, Cambridge, U.K. He is the Robinson Professor of Astronomy with the California Institute of Technology (Emeritus). After earning the B.Sc and B.Sc (Hons) degrees, in 1968 he joined the Cavendish Laboratory. He then spent five years as a Royal Society Weir Research Fellow with the